JOURNAL OF CATALYSIS 58, 337–347 (1979)

Mössbauer Investigation of Supported Fe and FeNi Catalysts

I. Effect of Pretreatment on Particle Size

G. B. RAUPP[1] AND W. N. DELGASS

School of Chemical Engineering, Purdue University, West Lafayette, Indiana 47907

Received July 13, 1978; revised January 9, 1979

Silica-supported Fe and FeNi catalysts show strong dependence of metal particle size on pretreatment, particularly the initial dehydration step. Room temperature Mössbauer spectra and supporting X-ray diffraction data reveal that mild pretreatment in the form of slow vacuum drying prior to reduction produces significantly smaller particles of Fe and FeNi on silica than either direct reduction or calcining. Once the catalyst precursor is completely dried, metal particles are relatively stable against further growth, suggesting that residual water or anions from the incipient wetness impregnation play a critical role in metal agglomeration during pretreatment. For 5 wt% Fe 5 wt% Ni on silica, vacuum drying and subsequent reduction produce FeNi alloy particles small enough to exhibit superparamagnetic behavior. Precalcining this catalyst increases the alloy particle size considerably as shown by a ferromagnetically split Mössbauer spectrum. Computer fitting of the broad peaks reveals significant amounts of metallic iron or extremely iron-rich alloy and, therefore, that phase separation can accompany particle growth in FeNi alloy catalysts.

INTRODUCTION

Iron has long been recognized as an important catalyst for the production of hydrocarbons from CO and H_2 (*1–9*). In fact, in the SASOL process, the only operating commercial process of its kind, fused potassium-promoted iron is used to catalyze Fischer–Tropsch synthesis (*10*). Previous research has revealed many interesting aspects of iron Fischer–Tropsch catalysts, including the importance of carbides (*9*) and changes in product distribution upon adding additional metals (*8*). In order to examine the nature and significance of carbide formation during reaction in more initimate chemical detail and to probe further the possibility of controlling selectivity to desired hydrocarbon products by alloying iron with other metals, we have begun a Mössbauer spectroscopic and kinetic investigation of supported iron-containing catalysts. This paper is the first of a series in which we report characterization of the chemical state of iron and iron–nickel alloy particles on SiO_2 by *in situ* Mössbauer spectroscopy before, after, and during reaction of H_2 with CO. We deal here with the nature of the catalyst before reaction.

The fine structural details of a supported metal catalyst depend on the complex chemistry of its genesis. Furthermore, certain reactions, including hydrogenolysis (*11*), isomerization (*12*), ammonia synthesis (*13*), and methanation (*14*, *15*), are known to be structure sensitive. Particle size strongly affects the structure of supported metals since changes in size can alter the

[1] Present address: Exxon Research & Engineering Company, Florham Park, N. J. 07932.

0021-9517/79/090337-11$02.00/0

distribution of exposed faces, surface irregularities, steps, and edges. In general, size controls both the number of special structural ensembles on the surface and the degree of coordinative unsaturation of individual surface atoms. In addition, smaller particles have a higher fraction of atoms in contact with the support and are, therefore, more susceptible to support interactions, an extreme example of which has recently been reported for group VIII metals on TiO_2 (*16*). Multiphase or alloy catalysts are particularly sensitive to dispersion (fraction exposed) if phase properties or surface enrichment are particle size dependent.

Clearly, the structural and chemical importance of particle size, as well as the obvious economy of metal utilization at small size, demand careful study of the variables that control particle size during catalyst preparation. Moss (*17*) has recently reviewed the effects of support, metal salt, and contacting method on catalyst properties. Effects of the salt used on particle size of iron catalysts have been probed with the Mössbauer effect(*18*). Bartholomew and Farrauto (*19*) have shown that the detailed chemistry of decomposition of nickel nitrate salt has a strong effect on dispersion for Ni/Al_2O_3 catalysts, while Dalla Betta and Boudart (*20*) have clearly demonstrated the crucial role of degree of hydration during metal reduction for Pt–Y zeolite.

In this work we have characterized the state of iron in Fe/SiO_2 and $FeNi/SiO_2$ catalysts as a function of pretreatment. The sensitivity of the Mössbauer effect to chemical state, magnetic ordering, and particle size of iron phases makes it well suited for such studies (*21*). Examination of effects of calcining, dehydration/reduction cycles, and effects of alloying on the resultant particle size of the iron phase shows a remarkable sensitivity of particle size to the severity of the initial dehydration process.

EXPERIMENTAL METHODS

Catalyst preparation. Iron and iron–nickel on silica catalysts were prepared via the incipient wetness impregnation technique. A known concentration of metal salt in water was prepared from Mallinckrodt analytical reagent grade nickel nitrate, $Ni(NO_3)_2 \cdot 6H_2O$, and/or ferric nitrate, $Fe(NO_3)_3 \cdot 9H_2O$. The salt crystals were dissolved in distilled water which has been further purified by deionization in a Barnstead high-capacity ion-exchange bed. The solution was then added to dry Cab-O-Sil EH5 silica, a high surface area ($\sim$400 m^2/g) support material composed of partially agglomerated microspheres of solid SiO_2 and obtained from the Cabot Corporation. The addition was accomplished dropwise with thorough stirring to promote even dispersion of the metal ions. Just enough solution was added to wet the entire surface, thus taking advantage of the surface spreading pressure of the solution to produce a uniform distribution of the ions. In the case of 10 wt% metal catalysts, 17.0 ml of solution was required for 9.0 g of silica (1.89 ml/g). The presence of ions from the metal salts significantly increased the solution's ability to wet the surface; fully 2.2 ml of deionized distilled water was needed to wet 1 g of silica.

Impregnated samples were air dried at room temperature for a minimum of 3 weeks, with daily stirring to ensure even drying. Preparation was completed by two different methods classified by the severity of pretreatment. In the first type, careful drying was achieved with a Thelco Model 19 vacuum oven. A liquid nitrogen trapped Welch Duo-Seal vacuum pump reduced the pressure to <1 kPa. The following heating schedule was used: 12–24 hr at 300°K, 2 hr at 353°K, 2 hr at 373°K, 2 hr at 393°K, and 16 hr at 413 °K. In the second type, air-dried catalysts were treated more harshly. Batches were calcined in 100 cc/min of UHP O_2 or 1% UHP O_2

in He at temperatures from 573 to 723°K for 6–24 hr.

Finally, dried or calcined catalyst powders were prepared for installation in the Mössbauer *in situ* cell (*22*) by pressing 0.1–0.4 g of powder at 8000 psi to make a 1.7-cm-diameter self-supporting wafer.

All catalyst compositions are reported on a dry, reduced basis as xFeyNi/SiO_2, where x and y are weight percents.

Experiments. Constant acceleration spectra are obtained with an Austin Science Associates, Inc. S-600 Mössbauer Spectrometer and a Reuter Stokes Model RS-P3-1605-261 proportional counter powered by a Fluke Model 415B dc supply. The detector pulses are preamplified by an Ortec Model 109PC preamplifier, amplified and shaped by a Canberra Model 1417B spectroscopy amplifier and selected by a Canberra Model 1437 timing single channel analyzer (SCA). The drive and counting electronics are interfaced with a Nuclear Data series 2200 multi-channel analyzer (MCA) equipped with a four input multiscaler. This setup is capable of accumulating greater than 100,000 counts/hr for 10 wt% Fe/SiO_2 samples.

The source was 50 mCi of ^{57}Co diffused into a rhodium matrix, obtained from Amersham Corporation. Absolute velocity calibration is determined with a 12.5-μm NBS Fe foil which gives linewidths of 0.23 mm/sec for the outer lines. Isomer shifts are reported with respect to this standard absorber. Computer analysis of the γ-ray data is made with a version of an Argonne variable metric minimization program, an iterative gradient algorithm to fit Lorentzian line shapes. Linear constraints of linewidth, dip, and/or position are employed to aid fitting only when they can be justified physically.

The stainless-steel absorber cell (*22*) has high purity Be windows for high γ-ray transmission. Using this cell, pretreatment or Mössbauer spectroscopy of catalysts can be accomplished at temperatures between 298 and 800°K, controlled to within ±1°K by a West Model 100 temperature controller. A multi-purpose gas handling system (Fig. 1) allows evacuation of the cell to $<1.3 \times 10^{-3}$ Pa or flow at 1 atmosphere of H_2, O_2, and He. All gases are UHP grade from Matheson. Hydrogen is passed through an Engelhard Deoxo, 10 ft^3/hr capacity, oxygen–hydrogen catalytic purifier and then through a fixed bed packed with drierite to remove water. Helium and oxygen are used without further purification.

A General Electric XJD-5 X-ray diffractometer provides X-ray diffraction patterns of the catalyst powders. Copper Kα radiation is measured with a scintillation detector. Reduced samples are passivated by flowing He over them at room temperature with gradual admittance over a 3- to 4-hr period of oxygen to the reduction cell until the partial pressure of O_2 is approximately 21%. Particle sizes are calculated from the line broadening of the diffraction pattern of the metal phase and the Scherrer equation. No diffraction lines from any iron oxide appear in the XRD patterns of the passivated samples. Iron and iron alloy foils are used to correct for instrumental broadening.

RESULTS AND DISCUSSION

Iron Catalysts

Samples of the same batch of air-dried 10Fe/SiO_2 catalyst were vacuum dried or calcined, loaded in the Mössbauer cell, and hydrogen reduced *in situ*. The room temperature Mössbauer spectra of the reduced catalysts, displayed in Fig. 2, have considerably different characteristic features showing that the chemical state of the catalyst is dependent on severity of pretreatment. Spectral parameters are summarized in Table 1. Figure 2a indicates that at least two forms of iron are present in the reduced catalysts. Most of the iron is represented by the paramagnetic asym-

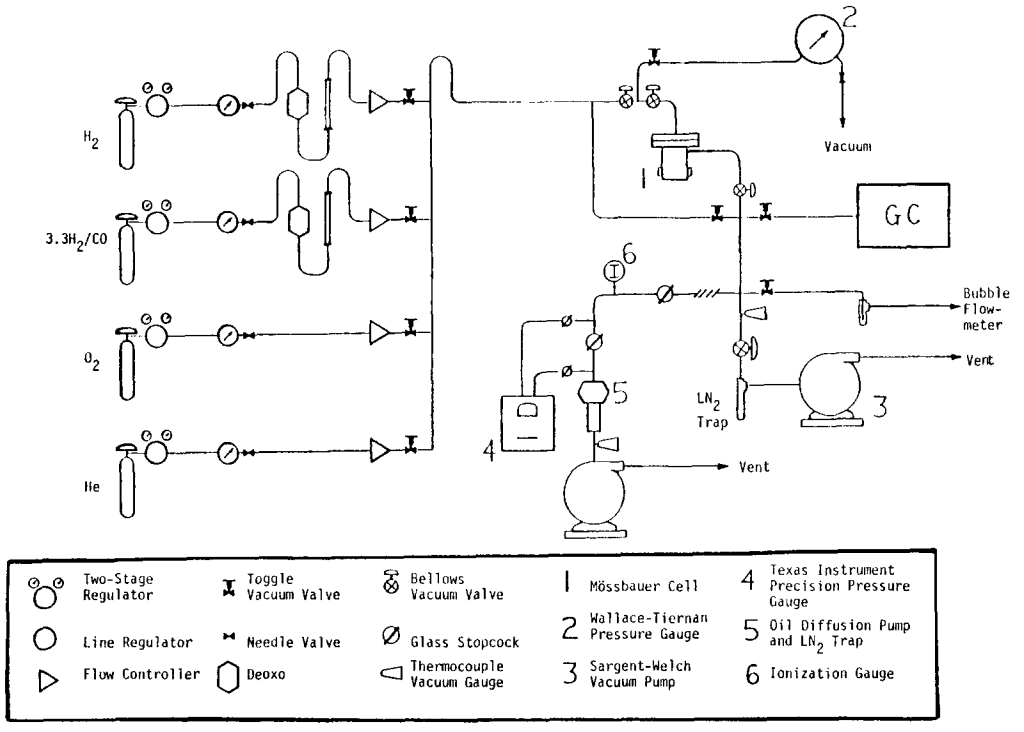

FIG. 1. Flow and vacuum system for Mössbauer absorber cell.

metric doublet, with a lesser contribution due to a phase corresponding to the six-line ferromagnetically split component. A 10-peak computer fit was employed with the positions of the two partially hidden peaks and the fully hidden peak of the six-line component constrained to have dip, width, and spacing consistent with the three visible peaks. The inner shoulder on the higher energy peak of the asymmetric central doublet led to a fit of this region with two superimposed doublets. Linewidths were constrained equal only in the central region of the spectrum. The computer-fitted splitting of the outer lines of the six-line component gives a hyperfine field (H) of 323 kOe, slightly less than the accepted value near 330 kOe for α-iron. The isomer shift (IS) near zero and the difficulty in fitting the poorly defined line shapes, however, warrant assignment of this component to metallic iron. Furthermore, previous Mössbauer studies have found that the magnetic field for small particles is less than that found for larger crystals of the same phase [see e.g. (*23*, *24*)]. Thus the observed decrease in the field suggests that the metallic Fe is well dispersed. The two superimposed central doublets are both assigned to ferrous species. The outer doublet has Mössbauer parameters typical of Fe^{2+} in bulk oxides. The inner doublet has a smaller isomer shift and quadrupole splitting, and is similar to peaks that have been observed in microcrystallites of FeO (*23*) and attributed to an Fe^{2+} species with coordination less than octahedral. This evidence for surface Fe^{2+} atoms suggests that the irreducible iron is also dispersed as small particles on the support.

In spectrum b (Fig. 2), reduction of the $10Fe/SiO_2$ catalysts was preceded by calcination at 648°K in flowing 1% O_2 in He for 24 hr. The qualitative spectral features are similar to those for the carefully dried catalyst, except that a much larger

portion of the spectral area is in the form of metallic iron. More severe calcination of the precursor at 723°K in flowing 1% O_2 in He for 24 hr gave a catalyst with essentially all of the iron in the zero-valent state after reduction (Fig. 2c). The fraction of iron in the reduced state for each of these three catalysts is estimated in Table 1.

We attribute enhanced reducibility of the iron as severity of pretreatment is increased to a concurrent increase in metal particle size. Several previous Mössbauer studies have shown that Fe on SiO_2 or Al_2O_3 at loadings of 0.1 to about 1 wt% is generally difficult to reduce; typically treatment in H_2 at 773°K for extended time cannot reduce the iron beyond Fe^{2+} (*24*, *25*). Stong interaction between iron in small particles and the support or actual ion-exchange of iron into the support surface account for this observed persistence of the ferrous phase. Reduction to Fe^0 generally can be achieved for loadings above 3%, or as particles become large enough to render strong support interaction unimportant by having a small fraction of the iron atoms in contact with the SiO_2 support. In the present case, 10% loading is sufficient to allow reduction to iron metal, but the degree of reduction is controlled by the amount of particle growth during pretreatment.

TABLE 1

Spectral Parameters for Reduced 10 Fe/SiO_2 Catalysts (Fig. 2)

Parameter	Spectrum		
	a	b	c
Internal magnetic field (kOe)	322.7	330.4	329.1
Isomer shift (mm/sec)			
Fe^0	+0.002	+0.001	+0.005
Fe^{2+}	+1.06	+1.05	—
Fe^{2+} [a]	+0.94	+0.84	—
Quadrupole splitting (mm/sec)			
Fe^{2+}	1.97	1.90	—
Fe^{2+} [a]	1.12	1.04	—
Fraction of Fe^0 [b]	0.150	0.673	1.00

[a] Assigned to surface ferrous species.
[b] Assuming arbitrarily that recoil free-fractions of the metal and the oxide are equal.

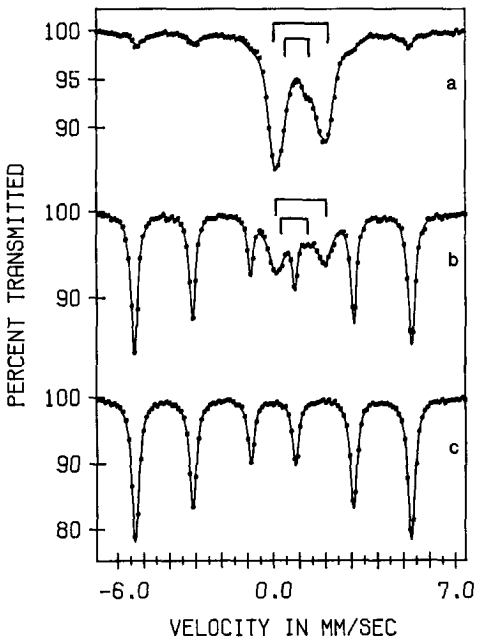

FIG. 2. Mössbauer spectra of reduced 10Fe/SiO_2 catalysts. (a) Vacuum-oven dried, reduced in H_2 24 hr at 723°K; (b) calcined in 1% O_2/He 12 hr at 648°K, reduced in H_2 8 hr at 723°K; (c) calcined in 1% O_2/He 24 hr at 723°K, reduced in H_2 8 hr at 723°K. All spectra were recorded in H_2 at room temperature.

Besides providing a measure of reducibility, the spectra in Fig. 2 yield limits for the metal particle sizes involved. The coupled spins in a magnetically ordered, single domain particle have preferred orientations in the microcrystallites. The relaxation time for flipping of spins from one preferred low-energy direction to another is given by the equation

$$\tau = \tau_0 \exp(KV/kT),$$

where τ_0 is a constant, K is the magnetic anisotropy barrier energy, V is the particle volume, k is the Boltzmann constant, and T is the absolute temperature. Thus at room temperature, a critical volume (diameter) exists, below which the relaxation time τ will be faster than the Larmor precession period of the nucleus. At this condition the average net spin in a given direction approaches zero and the magnetic

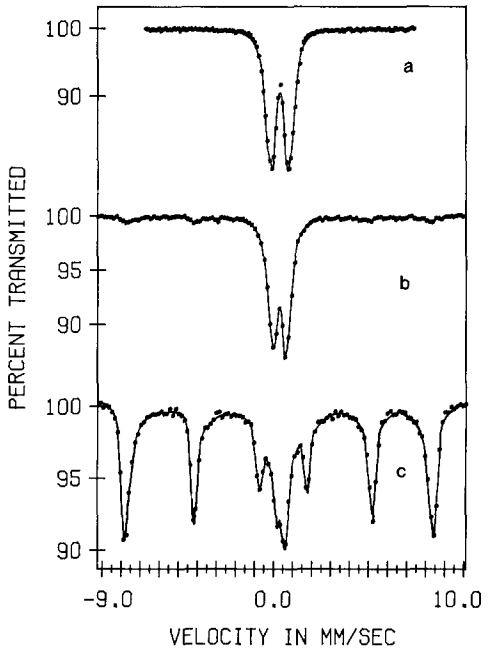

FIG. 3. Mössbauer spectra of oxidized $10Fe/SiO_2$ catalysts. (a) Vacuum-oven dried; (b) calcined in 1% O_2/He 12 hr at 648°K; (c) calcined in 1% O_2/He 24 hr at 723°K. All spectra were recorded *in vacuo* at room temperature.

structure changes from ferromagnetic to superparamagnetic. Small metallic iron clusters are well below the single domain size of 20 nm (*26*) for metallic iron, and thus have a single magnetization vector, **M**. Of the several sources of magnetic anisotropy, surface anisotropy can be particularly significant for small particles. Boudart and co-workers (*27*) have attributed their observation of six-line magnetically split iron spectra for particles as small as 1.5 nm to strong magneto-surface anisotropic effects. Thus the critical particle diameter (d_{cr}) for the onset of superparamagnetic behavior in metallic iron at room temperature is at least as small as 1.5 nm. For metal particles below d_{cr}, the six-line magnetic spectrum collapses into a single peak at 0.0 mm/sec. Computer fitting of the spectra in Fig. 2 showed in every case that addition of an extra unconstrained peak in the 0.0 mm/sec region is unnecessary. We conclude, therefore, that the average metallic iron particle size is greater than about 1.5 nm for each of the $10Fe/SiO_2$ catalysts studied. This may mean that very small iron oxide particles cannot be completely reduced when supported on SiO_2. In that case, Fig. 2 shows that the amount of iron in very small oxide particles decreases with severity of pretreatment.

Further information on the particle size of the metallic iron is available from spectrum a (Fig. 2) for the vacuum-dried catalyst. The breadth and slight asymmetry of the magnetically split lines, together with the decrease in observed hyperfine field, suggests that the average particle size is within a factor of approximately two of d_{cr} (*28*, *29*).

Mössbauer results for catalysts pretreated but not reduced provide estimates of the particle sizes for the larger iron particles. Kündig *et al.* [30] have shown that the critical particle diameter for superparamagnetic relaxation in α-Fe_2O_3 at room temperature is 13.5 nm. This higher value of the critical diameter reflects, of course, the fact that K is significantly lower for iron oxide compared to iron metal. As expected, the spectrum for vacuum dried $10Fe/SiO_2$ in Fig. 3a shows

TABLE 2

Spectral Parameters for Oxidized 10 Fe/SiO_2 (Fig. 3)

Parameter	Spectrum		
	a	b	c
Internal magnetic field H (kOe)	—	489.9	500.0
Isomer shift			
α-Fe_2O_3	—	+0.29	+0.30
Fe^{3+}	+0.47	+0.33	+0.35
Fe^{3+} [a]	+0.47	+0.32	+0.37
Quadrupole splitting ΔE_Q (mm/sec)			
α-Fe_2O_3 [b]	—	0.31	0.45
Fe^{3+}	0.69	0.53	0.50
Fe^{3+} [a]	1.22	0.97	0.61
Fractional magnetic area	0.0	0.13	0.72

[a] Assigned to surface Fe^{3+}.

[b] $\Delta_{12} - \Delta_{56}$, Splitting between lines 1 and 2 minus splitting between 5 and 6.

TABLE 3

Particle Size of $10Fe/SiO_2$ Catalysts

Pretreatment	Mössbauer spectroscopy (estimated) (nm)	X-Ray diffraction (nm)	Percentage exposed from XRD (%)
Vacuum dry T_{max} = 413°K 48 hr	<4.0	No observable peak	>20
Calcined at 648°K 12 hr	8.5- 9.0	7.9	10.8
Calcined at 723°K 24 hr	12.0–12.5	10.3	8.3

only a broad quadrupole-split doublet. Hence the average particle size is small enough that behavior is completely superparamagnetic. Direct calcining of the fresh catalyst in 1% O_2 in He for 12 hr at 673°K produces a particle size distribution with ~13% (based on spectral area) of the particles large enough to exhibit the ferrimagnetic behavior of α-Fe_2O_3, having a hyperfine field of 494 kOe, IS = +0.31 mm/sec, and identified as α-Fe_2O_3 rather than γ-Fe_2O_3 on the basis of the relatively large QS = 0.31 mm/sec (Fig. 3b). The spectrum for the catalyst calcined more severely at 723°K for 24 hr (Fig. 3c) shows that ~72% of the spectral area corresponds to α-Fe_2O_3 particles larger than 13.5 nm. Table 2 summarizes the spectral parameters for these samples.

The superparamagnetic component for each spectrum was fit with two sets of doublets. We assign the outer (wider quadrupole splitting) doublet to surface iron in keeping with the observation of Kündig *et al.* (*30*) that the quadrupole splitting of the Fe^{3+} doublet in very small α-Fe_2O_3 particles increases with decreasing particle size. Note that surface ferrous ions have lower splitting than bulk ions because the larger crystal field gradient is opposite in sign to the gradient of the iron d electrons (*31*). For high-spin ferric ions the d electron gradient is zero and the larger electric field gradient at the surface increases the quadrupole splitting. Size effects are also evident in the spectral component for the larger particles since the internal magnetic fields are lower than the 515-kOe value established for bulk α-Fe_2O_3.

X-Ray diffraction line broadening provides an independent measure of catalyst particle size for reduced and passivated samples. The values obtained by this method are expected to be somewhat low because passivation oxidizes the surface layer of the particles. The Mössbauer effect showed, however, that the amount of oxidation after passivation was about 25% at 80 Å and about 2% at 200 Å. If the oxide is a spherical shell around the metal core, it accounts for about 10% of the particle radius at 80 Å. This result, coupled with the absence of XRD lines for iron oxides, suggests that XRD line broadening provides a reasonable estimate of metal particle size. Table 3 shows good consistency between the particle sizes from X-ray diffraction and rough estimates of size obtained from the Mössbauer spectra by assuming that the relation between average particle size and percentage superparamagnetic spectral area is similar to that found for Fe/Al_2O_3 (*30*). Thus we conclude that increasingly severe precalcining increases Fe particle size.

This conclusion is particularly interesting in light of the observation that calcining affects particle size *only* if the fresh catalyst is hydrated. A sample which is first vacuum dried and then heated in O_2 or He or H_2 at temperatures up to 773°K for several hours prior to the final reduction treatment gives a spectrum identical to Fig. 2a.

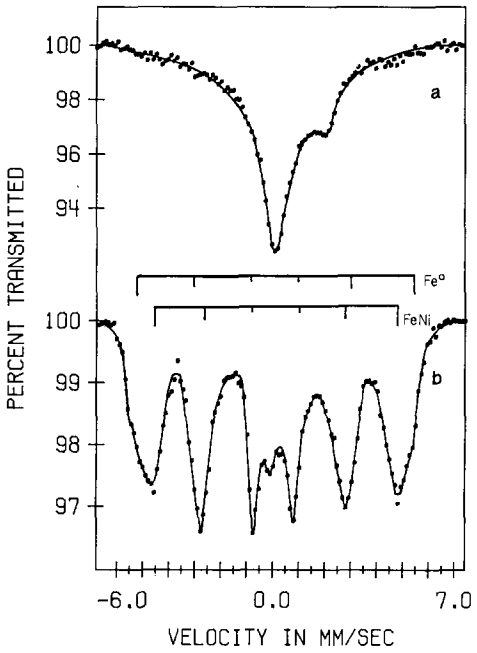

FIG. 4. Mössbauer spectra of reduced 5Fe5Ni/SiO_2 catalysts. (a) Vacuum-oven dried, reduced in H_2 8 hr at 723°K; (b) calcined in 1% O_2/He 6 hr at 573°K, reduced in H_2 8 hr at 723°K. Spectra recorded in He at room temperature.

This result strongly suggests that residual water or nitrate ions play an integral role in the metal agglomeration process.

Iron–Nickel Catalysts

The degree of alloy formation and effects of pretreatment have been examined for 5Fe5Ni/SiO_2, prepared by coimpregnation as described above. Spectrum a (Fig. 4) for this catalyst after careful vacuum drying shows that addition of a second metal to the catalyst drastically alters the chemical nature of the iron phase. No evidence of a magnetically split component characteristic of metallic iron exists. Instead, a broad single peak at +0.04 mm/sec dominates the spectrum. The non-Lorentzian line shape of this peak is unique to a magnetically ordered phase undergoing superparamagnetic relaxation and thus we assign this spectral component to small superparamagnetic particles of FeNi alloy. Another form of iron is present, as indicated by the shoulder on the high-energy side of the central peak. This shoulder is assigned to the right half of a ferrous quadrupole doublet.

The unique magnetic behavior of the FeNi system warrants care in interpreting spectrum a (Fig. 4). The variation of internal magnetic field with alloy composition, illustrated in Fig. 5, shows that bulk alloys of FeNi are not ferromagnetic across the full composition range. The internal fields in the BCC (low-Ni) and FCC (high-Ni) phases vary smoothly with composition but at about 30% Ni the field falls to zero. Alloys in this composition range are dubbed "Invars" because of their zero coefficient of thermal expansion at room temperature. Their anomalous magnetic and thermal properties are attributed to changes in magnetic ordering (*33*, *34*). Thus, for the FeNi system, interpretation of the observed single Mössbauer Fe line at room temperature is complicated since both the Invar composition at any particle size or superparamagnetic small particles with compositions away from the Invar region can exhibit this type of Mössbauer spectrum.

The isomer shift for bulk FeNi alloys varies only from 0.0 to +0.06 mm/sec with increasing Ni content and is +0.03 mm/sec at the Invar composition (*35*). Thus, while the measured value of +0.04 mm/sec is consistent with the nominal 50–50% FeNi composition, accurate phase identification cannot be made on this basis. Line shape was the key parameter in our assignment, since the line width of 1.5 mm/sec and abnormally wide wings are characteristic of a superparamagnetic peak and are significantly different from the width of 0.52 mm/sec and Lorentzian line shape reported for Invar (*36*).

Assignment of the spectrum a (Fig. 4) to small FeNi particles is supported by the behavior of the air-dried catalyst calcined in 1% O_2 in He at 573°K for

6 hr followed by reduction in H_2 (Fig. 4b). The large single peak of spectrum a (Fig. 4) is replaced by a magnetically split spectrum which can be fit by two overlapping sets of six lines. The major component is a broadened spectrum with H = 291 kOe and IS = +0.05 mm/sec. The data in Fig. 5 and a spectrum for a 50 wt% Fe 50 wt% Ni foil confirm that this phase is an FeNi alloy with nearly equal molar amounts of Fe and Ni. The broadening in this spectrum can come from a distribution of magnetic fields, corresponding to different numbers of Ni neighbors around the iron atoms in the disordered alloy, or from approach to the onset of superparamagnetism. A significant contribution of the latter effect is unlikely because the lines of the alloy foil have linewidths only slightly more narrow than those of the alloy catalyst. The second magnetic phase had narrow lines, an internal magnetic field near 330 kOe and a near zero isomer shift. This phase is attributed to metallic iron or an extremely iron-rich alloy.

The presence of two phases after particle growth (confirmed by XRD measurement) seems to be characteristic of this catalyst composition. Several attempts to generate a single phase, ferromagnetically split alloy were unsuccessful even when a different support, MgO, was used. The amount of the iron-rich phase corresponds roughly to the amount of unreduced iron in the small particle sample [spectrum a (Fig. 4)], but the structure of the two phase samples is not yet known.

Rapid heating of the air-dried FeNi catalyst precursor in hydrogen also causes agglomeration and phase separation. The spectrum of the air-dried sample consists entirely of superparamagnetic Fe^{3+}; two sets of overlapping ferric doublets fit the data. Vacuum drying and subsequent hydrogen reduction produces spectrum a (Fig. 4). Direct heating in H_2 gives a spectrum in which some paramagnetic alloy remains in the form of the small

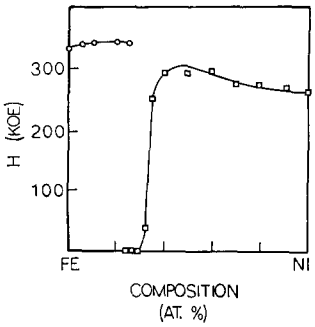

FIG. 5. Room temperature hyperfine magnetic fields for bulk FeNi alloys. Reproduced from Ref. (*32*) with permission.

central peak at IS ~ 0 mm/sec, but most of the iron yields a six-line magnetically split spectrum. The lines, broadened asymmetrically toward the center, are dissimilar to those for the disordered alloys and could not be fit with a simple combination of Lorentzians. The hyperfine field of ~330 kOe, measured at the maximum dip of the outer lines, indicates the presence of iron-rich particles. The peak asymmetry suggests a broad distribution of composition and, therefore, hyperfine field, although some superparamagnetic broadening (*28*, *29*) cannot be ruled out.

We note finally that as is the case for $10Fe/SiO_2$, metal particle growth in the $5Fe5Ni/SiO_2$ system is critically dependent on the initial dehydration procedure. Caresully dried samples do not sinter (based on Mössbauer and X-ray diffraction measurements) on subsequent heating in O_2, He, or H_2.

CONCLUSIONS

Mössbauer and supporting X-ray diffraction data show conclusively that the severity of pretreatment of an air-dried catalyst precursor affects the particle size of Fe and FeNi supported on silica. Since we have shown that particle growth is directly related to the presence of residual water or nitrate ions in the precursor, usual theories of sintering do not apply.

A number of interactions may influence agglomeration of metal ions during the final stages of drying. Water of hydration or nitrate ions bonded to the cation, as well as hydroxyl or nitrate groups on the support surface can alter the speed of surface diffusion. The rate of dehydration also plays a role. "Sudden" removal of water can spur precipitation of salts in larger pores while gradual removal of water can concentrate ions in the smaller pores, with final dehydration being controlled by capillary condensation. Nitrate decomposition begins at relatively low temperatures, near 413°K, but is probably not complete until much higher temperatures are achieved. Though nitrate decomposition undoubtedly plays some role in the genesis of the metal oxide particles and becomes more important as heating rate is increased the beneficial effect of vacuum drying at relatively low temperatures suggests that water removal prior to anion decomposition helps to anchor the metal ion to the support and prevents massive precipitation of salt particles in the pores. Though the mechanism of particle formation remains to be elucidated, a number of conclusions can be drawn from this work:

(1) Vacuum drying at mild conditions prior to reduction produces significantly smaller particles of Fe and FeNi on SiO_2 than does precalcining or direct reduction.

(2) After the initial drying step, particles are relatively stable against further growth.

(3) Fe and Ni form a nominally equimolar alloy in 5Fe5Ni/SiO_2 catalysts when vacuum drying precedes reduction.

(4) Metal particle growth can be accompanied by phase separation on 5Fe5Ni/SiO_2 catalysts.

ACKNOWLEDGMENTS

We gratefully acknowledge support of this work by NSF (Grant ENG76-20853) and the NSF Materials Research Program (Grant DMR76-00889A1), and thank E. M. Bild for contributions to the understanding of supported FeNi.

REFERENCES

1. Anderson, R. B., Hofer, L. J., Cohn, E. M., and Seligman, B., *J. Amer. Chem. Soc.* **73**, 944 (1951).
2. Storch, H. H., Golumbic, H., and Anderson, R. B., "The Fischer–Tropsch and Related Synthesis." Wiley, New York, 1951.
3. Fischer, F., and Tropsch, H., *Brennst.-Chem.* **7**, 97 (1926).
4. Stein, K. C., Thompson, G. P., and Anderson, R. B., *J. Phys. Chem.* **61**, 928 (1957).
5. Shultz, J. T., Karn, T. S., Bauer, J., and Anderson, R. B., *J. Catal.* **2**, 200 (1963).
6. Mills, G. A., and Steffgen, F. W., *Catal. Rev.* **8**, 159 (1973).
7. Anderson, R. B., *in* "Catalysis" (P. H. Emmett, Ed.), Vol. IV, pp. 1, 29, 257. Reinhold, New York, 1956.
8. Pichler, H., *Adv. Catal.* **4**, 271 (1952).
9. Hofer, L. J. E., *in* "Catalysis" (P. H. Emmett, Ed.), Vol. IV, p. 373. Reinhold, New York, 1956.
10. Dry, M. E., *Ind. Eng. Chem. Prod. Res. Dev.* **15**, 282 (1976).
11. Yates, D. J. C., and Sinfelt, J. H., *J. Catal.* **8**, 348 (1967).
12. Boudart, M., Aldag, A., Ptak, L. D., and Benson, J. E., *J. Catal.* **11**, 35 (1968).
13. Dumesic, J. A., Topsøe, H., and Boudart, M., *J. Catal.* **37**, 313 (1975).
14. Dalla Betta, R. A., Piken, A. G., and Shelef, M., *J. Catal.* **35**, 54 (1974).
15. Vannice, M. A., *J. Catal.* **40**, 129 (1975).
16. Tauster, S. J., Fung, S. C., and Garten, R. L., *J. Amer. Chem. Soc.* **100**, 170 (1978).
17. Moss, R. L., *in* "Experimental Methods in Catalytic Research" (R. B. Anderson and P. T. Dawson, Eds.), Vol. 2, p. 43. Academic Press, New York, 1976.
18. Rubashov, A. M., Fabrichnyi, P. B., Shakhov, B. V., and Babeshkin, *Zh. Fiz. Khim.* **46**, 1327 (1972).
19. Bartholomew, C. H., and Farrauto, R. J., *J. Catal.* **45**, 41 (1976).
20. Dalla Betta, R. A., and Boudart, M., *in* "Catalysis" (J. W. Hightower, Ed.), Vol. 2, p. 1329. North Holland, Amsterdam, 1973.
21. Delgass, W. N., Haller, G. L., Kellerman, R., and Lundsford, J. H., "Spectroscopy in Heterogeneous Catalysis." Academic Press, New York, 1979.
22. Delgass, W. N., and Chen, L., *Rev. Sci. Instrum.* **47**, 968 (1976).
23. Gager, H. M., and Hobson, M. C., Jr., *Catal. Rev.* **11**, 117 (1975).
24. Hobart, H., and Arnold, D., "Proceedings of the Conference on Mössbauer Spectroscopy"

(Tihany, 1969), p. 325. Akadémiai Kiadó, Budapest, 1971.

25. Malathi, N., and Puri, S. P., *J. Phys. Soc. Japan* **31**, 1418 (1971).

26. Morrish, A. H., "The Physical Principles of Magnetism," p. 344. John Wiley, New York, 1965.

27. Boudart, M., Delbouille, A., Dumesic, J. A., Khammouma, S., and Topsøe, H., *J. Catal.* **37**, 486 (1975).

28. Mørup, S., Topsøe, H., and Lipka, J., *J. Phys.* **37**, C6-287 (1976).

29. Mørup, S., and Topsøe, H., *Appl. Phys.* **11**, 63 (1976).

30. Kündig, W., Bömmel, H., Constabaris, G., and Lindquist, R. H., *Phys. Rev.* **142**, 327 (1966).

31. Ingalls, R., *Phys. Rev.* **133**, 787 (1964).

32. Johnson, C. E., Ridout, M. S., and Cranshaw, T. E., *Proc. Phys. Soc.* (*London*) **81**, 1079 (1963).

33. Window, B., *J. Appl. Phys.* **44**, 2853 (1973).

34. Tino, Y., and Arai, J., *J. Phys. Soc. Japan* **32**, 941 (1972).

35. Crowell, J. M., and Walker, J. C., *A.I.P. Conf. Proc.* **18**, 427 (1974).

36. Tomiyoshi, S., Yamamoto, H., and Hiroshi, W., *J. Phys. Soc. Japan* **30**, 1605 (1971).